Anomalous Absorption and Scattering of Short-Pulse High-Intensity Lasers in Underdense Plasmas

K-C. Tzeng and W. B. Mori
Departments of Physics and Electrical Engineering, University of California, Los Angeles, California 90095

C. D. Decker
Lawrence Livermore National Laboratory, Livermore, California 94550
(Received 11 September 1995)

The propagation of short-pulse lasers through several Rayleigh lengths of underdense plasma [$(1-4)\%\ n_{cr}$] is studied using multidimensional fully explicit particle-in-cell simulations. The simulations model 80 to 600 fs, 1 μm wavelength pulses in the intensity range of 1.5×10^{17} to 3.5×10^{19} W/cm^2. A detailed account is given for the energy lost out of the focal cone due to a combination of collective absorption and scattering losses. The figure of merit for the nonlinear transmission losses of a given pulse length is the amount of Raman forward scattering exponentiation within a Rayleigh length.

PACS numbers: 52.40.Nk, 42.25.Bs, 52.65.Rr

The interaction of radiation with matter is a fundamental subject of physics. The interaction between radiation and a neutral gas is relatively weak. This is illustrated by the fact that it takes 50 km of air at an atmosphere to Rayleigh scatter [1], and 1 km of atmospheric densities to Thomson scatter visible light. At the focal intensities ($I \geq 10^{17}$ W/cm^2) of short-pulse lasers matter is completely ionized. Therefore, at these intensities, laser-matter interactions are synonymous with laser-plasma interactions. In a plasma the classical absorption length for high-intensity visible radiation propagating through atmospheric densities is also on the order of a km [2]. However, it is well known that collective processes in an underdense plasma can significantly lower the absorption and scattering lengths. These processes include Raman backward (RBS), forward (RFS) [3], and side (RSS) [3–5] scattering, relativistic self-phase modulation (RSPM) [6], and relativistic filamentation [6]; as well as their whole beam analogs, self-modulation [7], hosing [8], and self-focusing [9]. Understanding these processes is essential for the successful development of plasma based accelerators [10], light sources [11], and the fast ignitor [12] fusion concept.

Previous investigations [5,7] were incapable of describing the highly nonlinear competition between these processes. Recently, two-dimensional (2D) particle-in-cell (PIC) simulations [13] showed the importance of Raman scattering at all angles, but these simulations were limited to small spot sizes and very short pulses. (RFS is the decay of a laser with frequency ω_0 into Stokes and anti-Stokes sidebands at frequencies $\omega_0 - \omega_p$ and $\omega_0 + \omega_p$, respectively, where ω_p is the plasma frequency.) Here, we use a parallelized, fully explicit PIC code, PEGASUS [14,15], which only models the region of plasma in which the laser pulse resides. As a result, we can model ongoing laser-plasma experiments in their entire spatial and temporal dimension in 2D for the first time. In a typical simulation, 1.2×10^7 particles are followed on an 8192×256 Cartesian grid for 3×10^4 time steps. We note that a Cartesian grid can underestimate the amount of self-focusing. On such a grid, we can model pulses up to $\tau_{FWHM} = 600$ fs and spot sizes of $w_0 = 18\ \mu$m propagating through several mm of plasma, assuming the laser wavelength is $\lambda_0 = 1\ \mu$m. Each simulation takes 150 CPU hours/processor on a 16-node IBM SP1 parallel computer at UCLA. A small sample of the results from this model have already been shown to be in agreement with measurements from a recent experiment [14].

In this Letter, we present results from simulations which cover a wide range of plasma densities [$n = (1-4)\%\ n_{cr}$, where n_{cr} is the critical density], pulse durations ($\tau_{FWHM} = 80-600$ fs), and peak intensities ($I \approx 1.5 \times 10^{17}-3.5 \times 10^{19}$ W/cm^2). The normalized vector potential of the laser is $a_0 \equiv eA_0/mc^2 = 8.5 \times 10^{-10}\lambda_0(\mu\text{m})\sqrt{I(\text{W/cm}^2)}$. In all the simulations w_0 is kept fixed, ions are immobile, and an s-polarized laser is focused to the edge of a uniform slab of preformed plasma. The parameters for these simulations are given in Table I. These simulations are directly relevant to several recent experiments [14,16]. In this table we have also provided the number of e-foldings of a square pulse for RBS during a pulse duration [17] [$G^{BS}(\tau_{FWHM})$] and for RFS at the back of the pulse after it has propagated a Rayleigh length [3] [$G^{FS}(x_R, \tau_{FWHM})$] where $G^{BS}(\tau) = [2(P/P_{cr})(n/n_{cr})^{-1/2}(c\tau/x_R)\,\omega_0\tau]^{1/2}$ and $G^{FS}(x,\tau) = [8(P/P_{cr})(n/n_{cr})(x/x_R)\,\omega_0\tau/(1 + a_0^2/2)]^{1/2}$. We have written these expressions in terms of x/x_R, $\omega_0\tau$, P/P_{cr}, and n/n_{cr}, where x is the distance the pulse has propagated into the plasma, $x_R = \pi w_0^2/\lambda_0$ is the Rayleigh length, P is the laser peak power, and P_{cr} is the critical power for relativistic self-focusing [9], $P/P_{cr} = a_0^2(w_0^2\omega_p^2/c^2)/32$.

The linear growth of RFS was investigated for short pulses in Ref. [13]. The main results of this Letter are that for these parameters the laser rapidly evolves

 0031-9007/96/76(18)/3332(4)$10.00

TABLE I. List of simulation parameters. In the simulation, letters L and S stand for long (600 fs) and short ($\leq$100 fs) pulses, the first number is % of $n/n_{\rm cr}$ and the second number is a_0. Each simulation is also identified as a single letter. Note that we have used the relativistically correct values for $P/P_{\rm cr}$ [9].

Runs	$\tau_{\rm FWHM}$	$n/n_{\rm cr}$	a_0	$P/P_{\rm cr}^{\rm 3D}$	$G^{\rm FS}(x_R, \tau_{\rm FWHM})$	$G^{\rm FS}(\tau_{\rm FWHM})$
A L_1_0.3	600 fs	1%	0.33	0.44	6.1	73
B L_1_0.8	600 fs	1%	0.8	2.2	12	110
C L_1.4_2	600 fs	1.4%	2	10	18	190
D L_2_0.8	600 fs	2%	0.8	4.4	24	130
E L_4_0.5	600 fs	4%	0.5	3.9	35	130
F S_1_0.8	100 fs	1%	0.8	2.2	4.8	19
G S_4_5	80 fs	4%	5	42	11	53
H S_4_0.8	80 fs	4%	0.8	8.9	17	21
I S_4_2	80 fs	4%	2	29	19	34

to a *nonlinear* state dominated by saturated levels of RFS, RSS, and self-focusing. This results in (15–70)% of the laser energy being lost from the focal cone in Rayleigh length distances. The figure of merit for these losses scales as $G^{\rm FS}(x_R, \tau_{\rm FWHM})$ for a given pulse length. Therefore, an atmosphere of gas will stop most high-intensity short-pulse lasers within mm distances.

To illustrate the highly nonlinear behavior of these pulses, we plot in Fig. 1 center slices of the laser's electric field envelope E_3 ($E_z \propto \sqrt{I}$) and the resulting plasma wave E_1 (E_x) after a 600 fs pulse has propagated a Rayleigh length ($x_R = 1$ mm for $w_0 = 18$ μm). In each plot the laser and its initial envelope are shown below the plasma wave. The left axis is for the laser, while the right axis is for the plasma wave. In Fig. 1(a) results from a 1D simulation with otherwise identical parameters to the 2D simulation L_1_0.8 are shown for comparison. This simulation demonstrates that 1D RFS can self-modulate a pulse. The onset of RFS occurs when a small notch develops in the pulse [13]. This notch can be caused by local pump depletion due to RBS (at all angles in 2D) which grows and saturates from wave breaking in a narrow region of the pulse, or from RSPM. The dominant **k** for RSPM is [6] $a_0 k_0/2$ which merges into ω_p/c when $a_0 = 2\omega_p/\omega_0$. Note that 113 e-foldings of RBS are possible for this case so that RBS grows and saturates during the rise time.

In Fig. 1(b) results from simulation L_1_0.8 are presented. Two-dimensional effects are apparent by comparing Fig. 1(b) with 1(a). In 2D the front of the pulse is more depleted, and the envelope is more severely modulated. This extra depletion is due primarily to three-wave and four-wave nonresonant RFS-RSS [3,5,18] at near-forward angles scattering light out of the pulse. Note that self-modulation [7] and hosing [8] are whole beam analogs of nonresonant RFS-RSS [3,18]. The modulations are more severe because the density depressions of the plasma wave focus light [7,13,18]. In addition, the RFS plasma wave amplitude is reduced because the RSS plasma waves generate a much hotter plasma upon wave breaking than RBS does alone. Large numbers of these energetic electrons are self-trapped, leading to wave breaking [13,19] (saturation) of the RFS plasma wave at a lower amplitude in 2D. The details of the self-trapped electron spectra will be given in a separate publication. We also note that when $P/P_{\rm cr} > 1$, portions of the pulse self-focus as seen in Fig. 1(b) where the laser intensity exceeds its original value by a factor of 3. In Fig. 1(c) results from simulation L_1_0.3 are presented. By comparing Fig. 1(b) to 1(c), the effect of lowering the laser intensity is clear. For this case $G^{\rm FS}(x_R, \tau_{\rm FWHM})$ is greatly reduced, and there are not enough e-foldings of RBS, RSS, or RSPM to seed RFS until the rear of the pulse. As a result the pulse is considerably more stable, as seen by the fact that the back of the pulse is just beginning to modulate due to RFS after propagating a Rayleigh length. In this case the plasma wave is below the warm wave-breaking limit [19], so no self-trapped electrons are generated within a Rayleigh length.

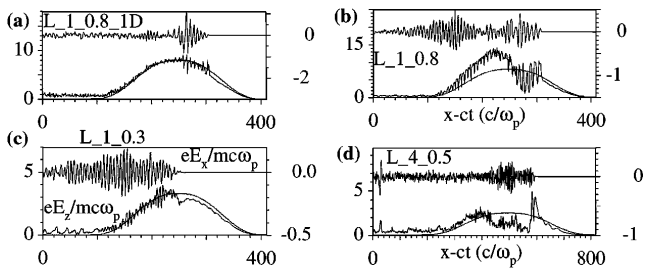

FIG. 1. Axial lineouts of the laser envelope and the plasma wave in units of $mc\omega_p/e$. (a) A 1D run with parameters identical to L_1_0.8, (b) L_1_0.8, (c) L_1_0.3, and (d) L_4_0.5. In all cases, $x = 1$ mm.

In Fig. 1(d) we show the consequences of increasing $G^{\rm FS}(x_R, \tau_{\rm FWHM})$. In this simulation the density has been raised to 4% $n_{\rm cr}$, while a_0 has actually been lowered to 0.5. The consequences of beam breakup are dramatic as a significant fraction of the pulse has been absorbed and side scattered. In addition, at the leading edge, the modulation at the k's for RSPM is clearly seen. The back of the pulse is diffusely side scattered by the turbulent wake generated by the leading edge. Eventually, the leading edge sharpens further, generating a coherent wake.

To further illustrate the nonlinear evolution of these intense pulses, we plot in Fig. 2 a sequence of color contours of the laser envelope for simulation L_1_0.8.

After propagating 0.32 mm into the plasma, RBS and RSS are beginning to occur in the rising edge as shown in Fig. 2(a). This causes laser energy to be scattered out of the pulse, causing the depletion of laser intensity shown on axis in Fig. 1(b). In those regions of the pulse where $P/P_{\rm cr} > 1$, the pulse acts like an optical fiber for the RSS Stokes radiation. Therefore, Stokes radiation at sufficiently small angles is reflected back into the pulse, causing the Stokes radiation to eventually evolve into a next lowest order symmetric Hermite-Gaussian mode. As a result, the Gaussian ansatz [7] is not sufficient to describe beam breakup in detail. We find that shorter pulses behave similarly to the leading edge of the 600 fs pulses. This is shown in Fig. 2(c), where the angle of the laser contours are similar to those in Fig. 2(a). RSS at this angle gradually erodes the back of the pulse, leaving a single beamlet λ_p long. The erosion is qualitatively similar to the results in Ref. [5].

In Fig. 2(b) we show that, after propagating 0.64 mm, the beam has self-focused to a spot size of a few c/ω_p with the central core undergoing RFS. In the 600 fs runs, no electron cavitation is observed. We emphasize that this is not due solely to the use of slab geometry but also to the occurrence of RFS. Cavitation is observed in runs S_4_2 and S_4_5, and in an otherwise identical run to $L\_1.4\_2$, where the x pusher in the code was turned off to suppress RFS-RSS. More details will be given in a separate publication. The angle of the laser envelope contours at the transverse edge corresponds to radiation leaving the pulse, indicating that not all the scattered light is confined as the beam focuses. The modulations to the laser envelope lead to similarly shaped contours in the plasma wave as shown in Fig. 2(b). Finally, after propagating 1.6 mm $\approx 1.6x_R$, a significant fraction of the pulse's energy has been absorbed into plasma waves and energetic particles as well as side scattered. The region of the pulse where RSS occurs at 0.32 mm is almost completely lost, while the back of the pulse undergoes the hosing instability. In this simulation the only noise source for hosing is the residual turbulence of the RFS and RSS plasma waves.

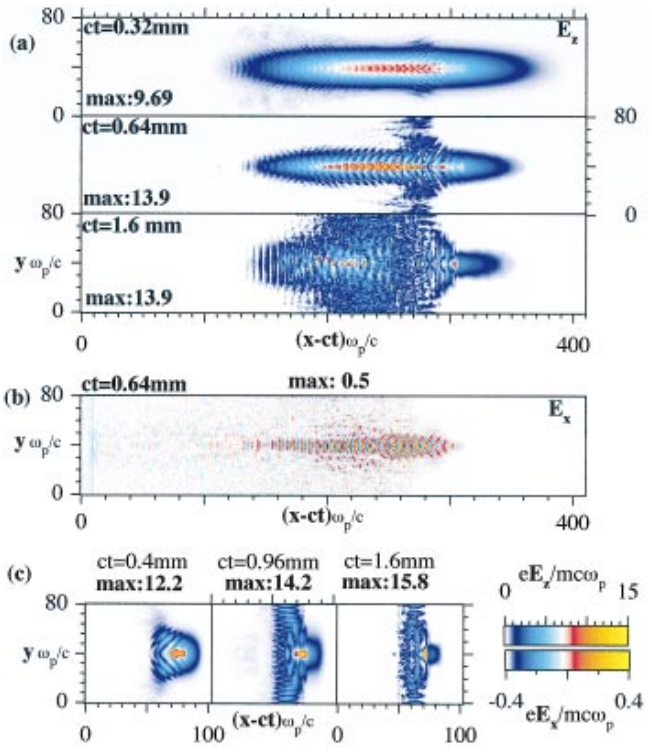

FIG. 2(color). Two-dimensional color contour plots for $L\_1\_0.8$ (600 fs) and $S\_1\_0.8$ (100 fs). (a) Evolution of the 600 fs laser pulse. (b) The plasma wave at $ct = 0.64$ mm. (c) Evolution of the 100 fs laser.

The importance of RSS is further illustrated in Fig. 3, where grey-scale contours of the lasers k spectra are shown at 0.64 and 1.6 mm. The cone angle for $f/8$ optics is shown because this was used in several of the recent experiments [14,16]. At 0.64 mm the dominant angle for RSS corresponding to the next higher order Hermite-Gaussian mode is still clear in the k spectrum. In addition, several Stokes and anti-Stokes sidebands for RFS are also apparent. This is clear in the center lineout as shown in Fig. 3(c) and 3(d). After 1.6 mm a considerable amount of light exists outside the focal cone, and multiple sidebands spaced at ω_p/c are apparent. The experimental detection of these multiple sidebands is clear evidence for RFS [13,14,18].

To quantify the importance of the nonlinear absorption and side scattering losses, we have calculated the normalized laser energy (electromagnetic) remaining in the simulation box and in an $f/8$ focal cone. It is difficult to separate the laser energy from other forms of energy, so we simply calculate $\varepsilon = \int E_3^2 dxdy$ where E_3 is due only to the laser for 2D slab geometry. In Fig. 4(a) $\varepsilon(x)/\varepsilon(0)$ is plotted for each simulation in Table I, where $1 - \varepsilon(x)/\varepsilon(0)$ is defined as the normalized absorption loss. The absorption is due to energy being transferred from the laser to plasma oscillations via RFS and energy being cascaded down to low frequency radiation which cannot keep up with the laser pulse. Note from Fig. 3(d)

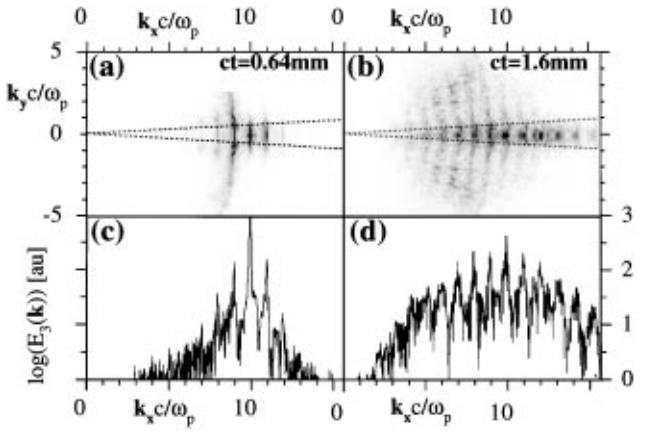

FIG. 3. Two-dimensional **k** spectra of the laser at (a) 0.64 mm and (b) 1.6 mm, and axial lineouts at (c) 0.64 mm and (d) 1.6 mm from simulation $L\_1\_0.8$.

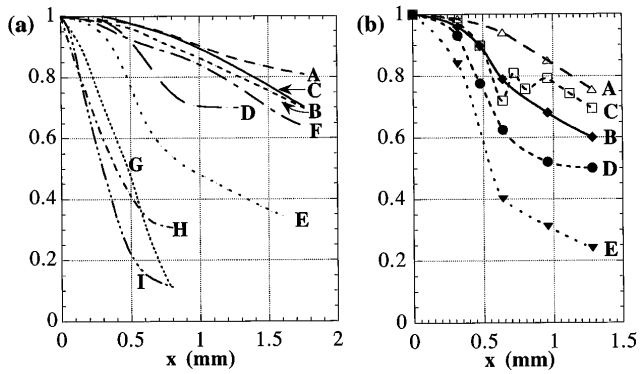

FIG. 4. The evolution of the electromagnetic energy left (a) in the simulation box and (b) in the $f/8$ focal cone. Both are normalized to the initial energies.

that the ratio of the energy left at the original frequency to $\varepsilon(0)$ is much less than $\varepsilon(x)/\varepsilon(0)$. RBS light will also leave the box, but, based on 1D simulations, we estimate this to be at most 5% over the 1.6 mm for these pulse lengths and plasma densities. Note in simulation $L\_2\_0.8$ the laser was sent through a finite 0.64 mm plasma slab so that the absorption curve begins to roll over after 0.64 mm. In Fig. 4(b) we subtract the additional laser energy which is scattered outside the focal cone for the long pulses. Therefore, this plot represents the total normalized transmission losses. For these pulse lengths the scattering losses are from 0.5 to 2 times the absorption losses. Note that the oscillation in Fig. 4(b) for $L\_1.4\_2$ is due to the dynamics of self-focusing which causes light at ω_0 to exist outside the original focal cone because of the reduction in spot size. From Fig. 4 it is clear that (15–70)% transmission losses of short pulses can occur within only 1 mm (a Rayleigh length) of very underdense plasma. These results are in agreement with previously reported experimental data [14].

An important observation is that both the normalized absorption and scattering losses tend to follow G^{FS} for a fixed pulse length (the spot size was fixed for all the simulations). This point is far from expected considering that G^{FS} represents the amount of linear exponentiation of one collective process while, as discussed earlier, the pulse's evolution is the result of the nonlinear competition between numerous processes. The exception is that $L\_1.4\_2$ has slightly less transmission losses than $L\_1\_0.8$.

The scaling of the absorption losses can be better understood by crudely equating the energy absorbed to that left in RFS generated plasma waves in the absence of wave breaking. The plasma energy is $(E_1^2/8\pi)A_p x$, where A_p is the cross-sectional area and it is assumed that the waves have been generated over the entire propagation distance. Dividing this energy by the pulse's energy gives the normalized absorption loss $(E_1^2/a_0^2)\,(n/n_{\mathrm{cr}})\,(A_p/\pi w_0^2)x/c\tau_{\mathrm{FWHM}}$, where $\underline{E}_1 = eE_1/mc\omega_p$. The scaling of this expression with a_0, w_0, and τ_{FWHM} is complicated because both $\underline{E}_1$ and A_p depend on these variables. However, if we assume that $\underline{E}_1$ and A_p depend insensitively on a_0, w_0, and τ_{FWHM}, then $1 - \varepsilon(x)/\varepsilon(0)$ should scale as $(1/a^2)\,(n/n_{\mathrm{cr}})\,(1/c\tau_{\mathrm{FWHM}})$ for a fixed x. Longer pulses have lower *normalized* absorption losses because they have more initial laser energy, and the energy given to the plasma is limited by the amount of plasma encountered. Therefore, the 5 ps ignitor pulse in the fast ignitor [12] could have low normalized absorption in the underdense channel; however, the scattering losses may still be significant. Note that the scaling with $1/a_0^2$ and n/n_{cr} is also rather consistent with the simulation results, e.g., $L\_1.4\_2$ has relatively less absorption loss. Note also that this scaling is the same as $G^{\mathrm{FS}}(x_R, \tau_{\mathrm{FWHM}})$ for $a_0 \gg 1$ because of relativistic corrections [3]. Furthermore, when $a_0 < 1$, $\underline{E}_1$ depends on a_0, and it is not constant within the pulse but $G^{\mathrm{FS}}(x_R, \tau_{\mathrm{FWHM}})$ still appears to determine the absorption loss.

We acknowledge useful conversations with Professor J. M. Dawson, Professor C. Joshi, Professor T. Katsouleas, and Dr. C. E. Clayton, Dr. E. Esarey, and Dr. P. Sprangle. We also want to thank the support from OAC at UCLA. This work was supported by DOE Grant No. DE-FG03-92ER40727 and LLNL Contract No. 4-444025-DA-26955.

[1] J. D. Jackson, *Classical Electrodynamics* (John Wiley & Sons, New York, 1975), 2nd ed., p. 423.
[2] C. D. Decker *et al.*, Phys. Plasmas **1**, 4043 (1994).
[3] W. B. Mori *et al.*, Phys. Rev. Lett. **72**, 1482 (1994).
[4] D. W. Forslund *et al.*, Phys. Rev. Lett. **54**, 558 (1985); D. W. Forslund *et al.*, Phys. Fluids **18**, 1002 (1975).
[5] T. Antonsen and P. Mora, Phys. Rev. Lett. **69**, 2204 (1992); N. E. Andreev *et al.*, JETP Lett. **55**, 571 (1992).
[6] C. E. Max *et al.*, Phys. Rev. Lett. **33**, 209 (1974); C. J. McKinstrie and R. Bingham, Phys. Fluids B **4**(8), 2626 (1992).
[7] E. Esarey *et al.*, Phys. Rev. Lett. **72**, 2887 (1994); P. Sprangle *et al.*, Phys. Rev. Lett. **69**, 2200 (1992).
[8] G. Shvets and J. Wurtele, Phys. Rev. Lett. **73**, 3540 (1994); P. Sprangle *et al.*, *ibid.* **73**, 3544 (1994).
[9] P. Sprangle *et al.*, IEEE Trans. Plasma Sci. **PS-15**, 145 (1987).
[10] Special issue, IEEE Trans. Plasma Sci. **PS-15**(2) (1987), edited by T. Katsouleas.
[11] Special issue, IEEE Trans. Plasma Sci. **PS-21**(1) (1993), edited by W. B. Mori.
[12] M. Tabek *et al.*, Phys. Plasmas **1**, 1626 (1994).
[13] C. D. Decker *et al.*, Phys. Rev. E **50**, R3338 (1994).
[14] C. A. Coverdale *et al.*, Phys. Rev. Lett. **74**, 4659 (1995).
[15] PEGASUS uses a parallelized version of the algorithm in ISIS.
[16] P. Monot *et al.*, Phys. Rev. Lett. **74**, 2953 (1995); K. Nakajima *et al.*, Phys. Rev. Lett. **74**, 4428 (1995); A. Modena *et al.*, Nature (London) **377**, 606 (1995).
[17] S. C. Wilks *et al.*, Phys. Plasmas **2**, 274 (1995).
[18] C. D. Decker *et al.* (to be published).
[19] T. Katsouleas and W. B. Mori, Phys. Rev. Lett. **61**, 90 (1988).